POLITECNICO DI TORINO
Repository ISTITUZIONALE

Graphene edge method for three-dimensional probing of Raman microscopes focal volumes

Original
Graphene edge method for three-dimensional probing of Raman microscopes focal volumes / Sacco, A.; Portesi, C.; Giovannozzi, A. M.; Rossi, A. M.. - In: JOURNAL OF RAMAN SPECTROSCOPY. - ISSN 0377-0486. - ELETTRONICO. - 52:10(2021), pp. 1671-1684. [10.1002/jrs.6187]

Availability:
This version is available at: 11583/2934565 since: 2021-10-26T11:24:00Z

Publisher:
John Wiley and Sons Ltd

Published
DOI:10.1002/jrs.6187

Terms of use:

This article is made available under terms and conditions as specified in the corresponding bibliographic description in the repository

Publisher copyright

(Article begins on next page)

25 April 2024

EDINBURGH INSTRUMENTS

50 YEARS 1971-2021

RMS1000
RAMAN MICROSCOPE

Extending the capabilities to Photoluminescence Microscopy, Time-Resolved Measurements and Fluorescence Lifetime Imaging (FLIM)

- Truly Confocal
- Five-Position Grating Turrets
- Two Spectrograph Options
- Up to Four Simultaneous Detectors

www.edinst.com

Check for updates

Received: 31 March 2021 | Revised: 14 May 2021 | Accepted: 7 June 2021

DOI: 10.1002/jrs.6187

RESEARCH ARTICLE

Journal of RAMAN SPECTROSCOPY WILEY

Graphene edge method for three-dimensional probing of Raman microscopes focal volumes

Alessio Sacco | **Chiara Portesi** | **Andrea Mario Giovannozzi** | **Andrea Mario Rossi**

Quantum Metrology and Nanotechnology Department, National Institute for Metrological Research (INRiM), Strada delle Cacce 91, Turin, 10135, Italy

Correspondence
Alessio Sacco, Quantum Metrology and Nanotechnology Department, National Institute for Metrological Research (INRiM), Strada delle Cacce 91, Turin 10135, Italy.
Email: a.sacco@inrim.it

Funding information
European Metrology Programme for Innovation and Research (EMPIR) (Funder ID: 10.13039/100014132); Horizon 2020 Framework Programme; EMPIR programme, Grant/Award Number: 19NRM04 ISO-G-SCoPe

Abstract

In this work, a layer of graphene was used as a standard material for the measurement of the dimensions of Raman microscopes focal volumes of different confocal Raman spectrometers equipped with different objectives and excitation laser wavelengths. This method consists in probing the volume near the focal point of the system by using a flat graphene monolayer sheet with a straight edge. Graphene was selected because of its high Raman cross section and mechanically and chemically stability, allowing fast measurements and easy manipulation. In this paper, a method to employ graphene to accurately and precisely measure the three dimensions of the focal volume of a Raman microscope is presented; scanning along the axial and lateral directions, it is possible to reconstruct the three dimensions of the focal volume. Furthermore, these operations can be combined in a single procedure which allows the measurement of projections of the volume on planes parallel to the optical axis. Knowledge of these parameters enable absolute quantification of Raman-active molecules and support high-resolution Raman imaging.

KEYWORDS

dimensional analysis, focal volume, graphene, metrology, quantification

1 | INTRODUCTION

Raman microspectroscopy is a measurement technique that allows its growing community to rapidly detect and identify chemical species. Raman spectroscopy is a versatile method that nowadays is widespread in both industry and research, spanning such diverse fields as physics, chemistry, biology, art, pharmaceutical industry, medical analysis and more.[1–8] Along with most of its related variants, such as surface-enhanced Raman spectroscopy (SERS),[9–12] it allows fast, non-destructive, label-free chemical identification analysis of solid, liquid and gaseous samples. When conveyed by an optical microscope, Raman microspectroscopy with visible light excitation is capable of reaching submicrometric spatial resolutions,[13,14] and two- and three-dimensional chemical imaging is easily carried out with the adoption of motorised stages, allowing widespread analytical industrial and research applications, from the study of the distribution of active molecules in pharmaceuticals to the characterisation of the different layers in multilayered packaging materials, materials science fundamental

This is an open access article under the terms of the Creative Commons Attribution-NonCommercial License, which permits use, distribution and reproduction in any medium, provided the original work is properly cited and is not used for commercial purposes.
© 2021 The Authors. *Journal of Raman Spectroscopy* published by John Wiley & Sons Ltd.

studies and industrial quality control. Also, in biological application, the Raman imaging could play a crucial role, for example, for the detection and characterisation of shape and size of bacteria and the monitoring at morphological level of the interaction with antibiotics.[15–17]

The three-dimensional geometry characteristics of the focal volume of Raman microspectrometers, especially the spot size at focus and the focal depth, are parameters that vary according to the specific experimental conditions (e.g., laser wavelength and type, objective, alignment and confocal aperture size) which are fundamental both for unbiased Raman imaging and for accurate substance quantification. While primarily employed for the detection and identification of chemical compounds in many matrices and phases, Raman spectroscopy can be a tool for the quantification of substances as well. Nowadays, this is generally accomplished with calibration methods undertaken with the measurement of known quantities of the considered analyte and the study of the spectral intensities of the calibration samples as a function of the amount of substance (i.e., mass, ratios, analyte concentration and number of units or layers), usually by utilising univariate or multivariate regression models.[18–20] Nevertheless, this kind of quantitative measurement has limited scope, as it is neither absolute nor metrologically traceable to the International System of Units (SI) per se: absolute, traceable quantification with Raman spectroscopy is still an unachieved and much-sought objective in this field.

In order to obtain correct information on the spatial features of a spectroscopic image captured with an optical microscopy apparatus and to achieve a quantitative measurement with such a setup, accurate knowledge of the dimensions of the investigated area or volume is of utmost importance, and to do so, not only a value for the measurand must be sought but also its uncertainty needs to be appropriately estimated.[21,22] In principle, these parameters may be somewhat predicted by analytically calculating them on the basis of the specifications of the instrumental apparatus, as well-known formulae exist for this purpose.[23–25] However, non-ideality of the operational parameters (e.g., faults of the apparatus components and changes of environmental conditions or misalignments due to fluctuations or drifts of the equipment) is expected, and it is laborious, when not impossible, to verify. These factors can dramatically change the experimental conditions with respect to theory and expectations. Lack of information on components of the calculation of the dimensional features of the focal volume makes an unbiased estimation an implausible endeavour, with a high risk of lack of accuracy and/or gross misestimation of the uncertainty on the final result. This is furtherly complicated by the fact that the radiation intensity distribution and its collection efficiency around the focal point are not uniform and do not present definite limits per se but have a continuous three-dimensional profile that theoretically never reaches zero; hence, conventions should be established. For these reasons, the possibility of having experimental values with associated uncertainty to be used for calibration purposes, proficiency testing, interlaboratory studies or production certified materials is of paramount importance.

With the goal of supporting optical micro-imaging dimensional analysis and the achievement of the possibility of quantification with Raman spectroscopy and its related techniques, in this paper, a novel method for the accurate three-dimensional spatial measurement of the focal volume of Raman microscopes is introduced and applied to real instrumental systems. This kind of procedure is usually based on the probing of the focal volume by employing a Raman scatterer with small but known physical dimensions as a sample, shifting its position near the focal point of the apparatus and analysing the arising Raman intensity as a function of its position. Here, a novel procedure is presented for the characterisation of the spatial profiles of the focal volume of a Raman microspectrophotometer in three dimensions employing an asymmetric graphene structure: the 'graphene edge' method. This approach was applied to two different confocal Raman microscopes and with two different excitation laser wavelengths. The process consists in the Raman measurement of the straight edge of a planar flake of graphene while scanning it in the desired directions. This results in dimensional profiles of the focal volume along those directions from which a three-dimensional mapping of the volume can be extrapolated, with a precision limited only by the scanning method itself.

Graphene is a very appropriate material for this kind of investigation, as it is very commonly studied by Raman spectroscopy, and its spectrum and behaviour in many measurement conditions are well known. As a carbon allotrope, it has a high Raman cross section; also, it has high thermal conductivity, and it is not easily damaged by focussed visible radiation. Graphene attracted extensive interest of the scientific community in the past years, and nowadays, large-area, relatively pure samples of monolayer graphene can be inexpensively produced or purchased. The most prominent Raman signals of monolayer and few-layer graphene are described below. The G peak is located near 1580 cm^{-1}, and its position and especially its relative intensity in the spectrum vary according to the number of layers, and it arises from the carbon pairs in-plane stretching. This band is known to split into two band, G+ and G−, when the graphene sheet is subject to strains or curvature. The 2D signal (also called G′),

located at approximately 2670 cm^{-1}, is due to double-phonon scattering and corresponds to the graphene breathing mode, and in single-layer graphene, it has a Lorentzian shape; if the number of layers is two or more, the band shape is instead the convolution of more Lorentzian curves. In defect-free monolayer graphene, the 2D/G band intensity ratio is approximately 2; therefore, the 2D peak is the most intense signal. When the graphene presents structural defects such as lattice disorder or sheet edges, the D band, which is the single phonon mode corresponding to the 2D signal, is active at ~1350 cm^{-1}, with the D/G bands intensity ratio increasing with the density of defects in the lattice. Graphene with a high density of defects also presents the D′ band, a signal at approximately 1620 cm^{-1} that is less intense than the D peak and that is usually convoluted with the G band, as well as a D + D′ band near 3000 cm^{-1}. The positions of the aforementioned signals in the Raman spectrum also depend on measurement conditions such as excitation wavelength and temperature.[26]

2 | THE GRAPHENE EDGE METHOD

In this work, the focal volume characterisation of different Raman microspectroscopy setups was carried out by employing a nanostructured feature (the edge of a graphene flat sheet) as a probe and by measuring its Raman spectrum while shifting it in varying directions near the focal point, inside and around the focal volume. An effective sample for spatial measurements of this kind should have the smallest possible dimension along the scan direction, as a large one results in broadening of the measured feature due to the probe dimensions convolution with the measurand.[13,14,27–31] Furthermore, especially because of the advisable small scale of the scatterer, a material with a high Raman cross section is desirable to reach an adequate signal to noise ratio of the spectra. This also allows to reduce measurement times, which could translate into sources of uncertainty on the final result in themselves because of possible mechanical and thermal drifts of the sample and the microscope stage, instability of the laser power, external vibrations and other changes in the measurement conditions that acquire more weight, the longer the scan is prolonged.[27,32,33] For these reasons, single-layer graphene is an ideal material for this purpose: it has some of the smallest possible dimensions because of its atomic thickness, and it is very Raman active as well. Furthermore, it is quite chemically stable, and it is a good thermal conductor that is therefore able to withstand relatively high excitation power densities without being modified or damaged. Moreover, its Raman profile is well known and easily analysable, and it exhibits relatively high absorbance of visible light (a graphene monolayer absorbs about 2.3% of visible incident white light[34]), which is a very convenient property in order to locate it with optical microscopy and for the manipulation of the sample.[35] The employment of a graphene sheet for depth profiling of Raman microscopes was recently realised,[13,28] and carbon-based nanomaterials such as carbon nanotubes (CNTs)[13] and nanostructures such as polystyrene nanobeads[36] were employed for beam waist planar measurements of Raman microspectrometers (in the latter solution, certified reference materials could be used). For the first time, this work shows how graphene itself could be utilised to characterise both lateral and axial dimensions of the focal volume of such an apparatus. This has the advantage of making it possible to employ a single sample to probe all its dimensions, and even two of them with a single three-dimensional scan, while analysing the same Raman signal: such analysis reduces biases due to different spectral processing due to different signal to noise ratios, Raman peak shape, and so forth. In addition, the same material employed to probe the volume may also be easily characterised dimensionally, for example, through atomic force microscopy (AFM), and chemically, for example, through Raman spectroscopy itself, scanning tunnelling microscopy (STM) and energy dispersive X-ray spectroscopy (EDX), before use, paving the way towards metrological traceability in Raman microscopy.

The optical system of the microscope is expected to have at least some degree of rotational symmetry around the optical axis, that is, the line parallel to the direction of propagation of the light beam on which the ideal focal point lies. Therefore, the procedures for probing the dimensions of the focal volume of a Raman microscope with graphene edge are different whether the axial dimension (parallel to the optical axis) or lateral dimensions (the dimensions of the spot size or beam waist, a section of the focal volume perpendicular to the optical axis) are sought.

Figure 1 shows a scheme of the procedure to map the axial dimensions of the focal volume. First, an area of the sample entirely covered in graphene is located, far from the limits of the graphene sheet, hence ascribable to a complete layer. The actual minimum distance from the edge(s) of the graphene flake depends on the width of the beam waist and the numerical aperture of the objective: obviously, for the measurement to be accurate, the focal volume should be sectioned by a full graphene sheet throughout the whole scan. After the area is selected, the sample is brought into focus by maximising the signal intensity of its chosen Raman band (the 2D

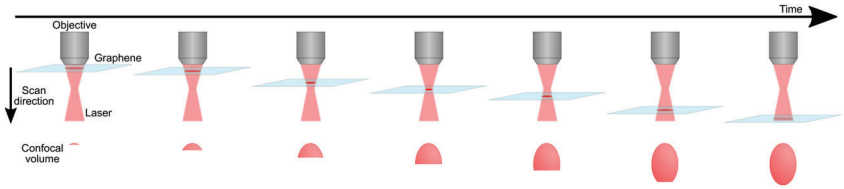

FIGURE 1 Scheme of the probing of the axial dimension of the confocal volume of a Raman microscope by a graphene layer. An area of the graphene sample away from the edge is scanned along the optical axis near the focal point, whereas its Raman spectrum is acquired at multiple times. An intensity profile in that direction can be reconstructed by monitoring the intensity of the graphene Raman signal (in figure, the volume is extrapolated on the basis of a circular spot at focus) [Colour figure can be viewed at wileyonlinelibrary.com]

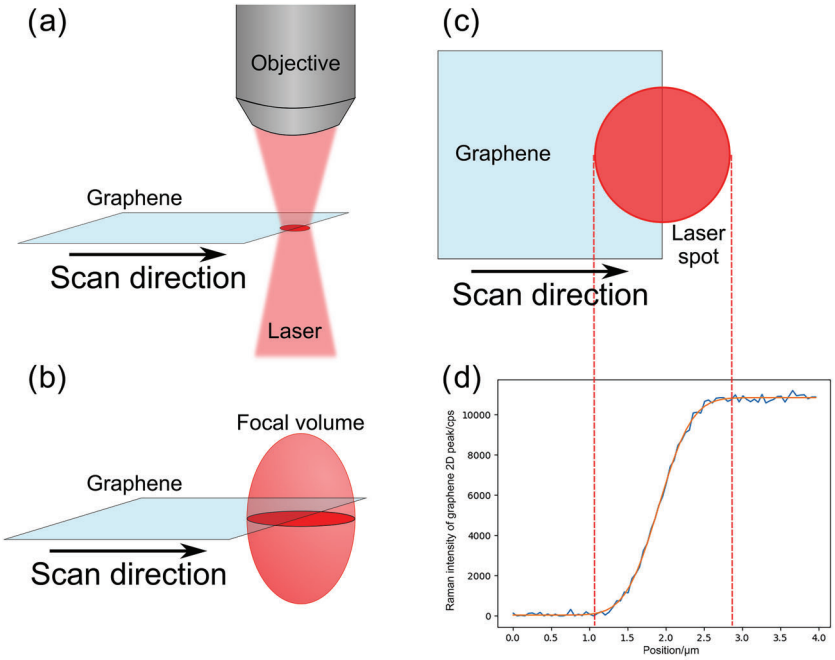

FIGURE 2 Scheme of the graphene edge method for the measurement of the width of the focal volume and the spot size at focus. (a) General geometry of the system during measurement: the edge is scanned along a plane normal to the optical axis, whereas its Raman spectrum is measured. (b) Apparatus with the focal volume of a confocal microscope depicted (darker red indicates the spot size at the focal plane). (c) Planar view. (d) Result of the scan, which is a Raman intensity profile along the scan direction (blue line: Experimental data; orange line: Cumulative Gaussian function least-square regression) [Colour figure can be viewed at wileyonlinelibrary.com]

peak is the recommended choice, more on that below), and experimental parameters are optimised to reach a good compromise between signal intensity and scan duration. A scan position interval around this point is then decided, according either to the expected depth of focus or to the variation of the Raman signal while moving the sample along the axis: in the latter case, it is advisable to include the interval in which the Raman signal is at least 10% of its maximum at focus.

It is not possible to measure the width of the focussed beam using a full graphene sheet: from this need, the graphene edge method arises. This procedure was inspired by the widespread knife edge method for the determination of beam width of unfocussed or loosely focussed lasers, which is routinely being employed for decades.[37] The important differences are that the graphene edge method is highly precise, it requires no external tools apart from the sample itself, it is independent from operator skill and it actually yields Raman information for the system. By having a sample with a definite structure along the lateral dimension, this can be scanned orthogonally with respect to the optical axis to acquire information on the beam width on that plane. In particular, a straight graphene edge scanned near the focal point and perpendicularly to both the optical axis and the edge itself results in a spectral profile which is simply the cumulative function of the profile of the spot, that is, the integral of the profile function between infinity and that position of the edge, along the scan direction. In Figure 2, a schematisation of the procedure is shown.

Many applications of Raman microspectroscopy, especially Raman imaging and any attempts at substances quantification, require the definition of either a spot size at the focal plane or a complete focal volume. However, much like the profile of a laser beam,[23,38] the focal volume of a microscope has no exact bounds, and in ideality, the profile has a non-zero intensity throughout the whole real domain.[24] Therefore, an unequivocal definition of the width, depth and therefore volume of focus is impossible without establishing conventions. Depending on the application, the most commonly

accepted boundaries are the following: (a) the points where the intensity is reduced by a factor of $1/e^2$ (where e is Euler's number) with respect to the maximum (for a Gaussian profile, this translates in limiting the curve to two times its width parameter σ in each direction, with an intensity threshold of 13.5% of the maximum: such interval contains 95.5% of the total integral); (b) the full width at half maximum (FWHM) of the profile or (c) either the Rayleigh criterion or the Abbe criterion.[23,38–40] The Rayleigh and Abbe criteria simply employ the radiation wavelength and the numerical aperture of the instrument and are not applicable in measurements of profiles, as they only describe ideal cases. In order to apply the other two conventions, it is required to estimate the aforementioned data from profiles. To determine the beam waist, the focal depth and the position of the focus point of the apparatus, and to interpret the data produced by these measurements, regression analysis on the profile is necessary, instead of applying the criteria directly on data. This is aimed also at reducing uncertainty and at compensating the likely noisy/non-zero baseline, the higher oscillations in Raman signal at high intensities,[41,42] and the possible vibrations, drifts and general non-ideality of the scanning system. The point-spread function (PSF) of an aberration-free microscope objective with a circular aperture, which can be idealised and approximated as a radially symmetric ideal optical lens, is in any case limited by diffraction due to the edges of the aperture (i.e., the sides of the idealised lens). Therefore, the lateral intensity profile of a monochromatic radiation focussed by said objective is described by the Airy function in the radial direction, yielding the pattern known as Airy disc at the focus plane. A similar intensity profile is shown along the optical axis for a confocal microscope, albeit this axial distribution is much wider than the lateral one (this is the reason for the lower spatial resolution of confocal optical imaging in the axial direction). Given the cylindrical symmetry of the system, tracing the limit of the confocal volume using an intensity threshold an ellipsoid with a circular section is obtained.[24,43] A widely accepted approximation of the Airy function in optics is the Gaussian function,[44] which will be employed throughout this work instead. This is a convenient function to work with, and it is generally used in fluorescence and Raman quantification and mapping, because Gaussian integrals and parameters are very well known or calculated/tabulated, and Gaussian regressions routines are easily available for data analysis. It is especially welcome in the case of the graphene edge probing method, because the cumulative function required for profile best fitting, with this approximation, is a simple variant of the common Gauss error function $erf(x)$.

The measurement methods presented in this paper answer criticalities deriving from several factors that exist in real microspectroscopy systems which may result in severe differences with respect to the ideal case by identifying and measuring them. For example, optical aberrations are commonly present in real microscopes, due to misalignment, drifts or apparatus imperfections, that may produce a noticeable departure from cylindrical symmetric geometry; therefore, scanning more than one diametrical direction is advisable. Furthermore, laser sources themselves are not ideal; hence, measurements with one source are not necessarily extensible to different sources, even after applying a scaling factor for wavelength, which is why they are accurately applicable only to the specific setup, that is, that particular combination of laser source, microscope objective and medium, as aligned at the time. Moreover, in many optical systems, a sizeable portion of the uncertainty derives from the sample motor stages, which can have incongruous performances along different directions, or varying according to the position of the sample relative to the stage area, to the scan speed, and so forth; because of this, considerable care must be put into the choice of the probing parameters, on the grounds that slow scanning speeds may influence the stability of some types of stages, whereas acquisition times which are too rapid would yield spectra with low signal.[27,28,30,31,40]

The graphene edge method can also be employed in an alternative procedure which integrates axial and radial profiling. Modern Raman microspectrometers, in fact, allow multiple planar scans at different coordinates, allowing three-dimensional mapping. Using this kind of feature to scan the graphene edge at different focal planes (multiple scans on each plane can be performed, then averaged) results in a two-dimensional image which is effectively the projection of the focal volume on the scan plane. This approach, while requiring a longer time to complete, has the advantage of resulting in an actual measurement of the Raman intensity distribution along optical planes other than the focal plane. As a result, this method allows to go beyond the extrapolations required to define the dimensions of the focal volume by deriving them from a series of profiles intersecting the focal point or plane by acquiring actual two-dimensional images of the whole focal volume.

3 | EXPERIMENTAL

In this work, the graphene edge method was applied to several experimental configurations on two different dispersive confocal Raman microscopes: an unmodified

commercial DXR™xi Raman Imaging system, from Thermo Fisher Scientific™, and a custom setup assembled with a DXR™ Raman spectroscope (by Thermo Fisher Scientific™) with an optical path modified to pass through a Ntegra™ scanning probe microscope (SPM), by NT-MDT®; the latter is in fact a tip-enhanced Raman spectroscopy (TERS) apparatus,[45,46] although for these measurements the Raman-enhancing probe was not mounted in order to employ it as a simple confocal Raman microscope. The DXRxi features a magnetic sample stage with a step size of $(0.1 \times 0.1 \times 0.2)$ μm along the three Cartesian axes ($x \times y \times z$), where z is the direction of the optical axis. The Ntegra is equipped with a piezoelectric tube stage with capacitive sensors for bias correction, allowing a maximum travel of $(90 \times 90 \times 9)$ μm; this kind of positioning device is common for SPM and allows the technique to reach spatial precisions in the order of the nanometre. In the conditions, they were used in this work; both spectrometers have spectral resolutions of 5 cm^{-1}, spectral steps of 2 cm^{-1} on average and spectral windows of [50; 3500] cm^{-1}.

Two excitation sources were utilised in the study: a 632.8 nm He-Ne laser that could be employed on both spectrometers and a 532 nm, frequency-doubled Nd:YAG laser on the DXRxi only. The microscope objectives were an Olympus™ 100× (Olympus MPLN100xBD) with a numerical aperture (NA) of 0.9 and a focal length of 1.8 mm mounted on the DXRxi, and a Mitutoyo™ 100× (Mitutoyo M Plan Apo 100×) long-working distance (LWD) with 0.7 NA and a focal length of 2 mm used on the DXR-Ntegra apparatus. All measurements were performed in air, in environmental conditions. The combinations of laser wavelengths, microscope objectives and stages that were used for this study can be summarised into three different configurations. The DXR-Ntegra, (piezoelectric stage, 100×0.7 NA LWD microscope objective) was employed with the 633 nm He-Ne excitation laser; both the 633 nm and the 532 nm Nd:YAG lasers were employed on the DXRxi (magnetic stage, 100×0.9 NA objective). Unless specified, a 50 μm diameter pinhole was utilised as a confocal aperture during measurements.

The piezoelectric SPM stage was calibrated via the measurement by AFM of a three-dimensional length standard grating.[27] Both Raman spectrometers underwent spectral calibration both for frequency and intensity: spectral frequency was calibrated through measurement of the emission lines of a low-pressure neon lamp and verified with Raman measurement of a polystyrene standard reference material, whereas intensity calibration was achieved by white light-emitting diode (LED) spectral measurement.

The graphene edge sample was produced by transfer from the native substrate[47] to a monocrystalline silicon wafer with 280 nm of thermally grown silicon oxide on the surface, because this support surface was deemed to yield optimal contrast between graphene-covered and uncovered areas in order to easily locate the edge with optical microscopy before measurement.[35] The production started from commercially available CVD monolayer graphene grown on copper.[46] A thin layer of polymethyl methacrylate (PMMA) was first deposited by spin-coating on the graphene as a support; then, the copper surface was etched completely; the PMMA was then laid out on the SiO_2/Si wafer, and after thermal annealing, the PMMA was dissolved in acetone, resulting in wide areas (more than 10 μm for each side) of graphene. A suitable graphene edge was then located, and AFM was performed on it to verify the straightness of the edge and to quantify the difference from an ideal straight edge. Because both microspectrometers work in a 180° backscattering geometry and the chosen substrate was not transparent, the graphene-covered side of the sample faced the objectives during the experiments. Other types of substrates (e.g., transparent supports if needed) could be employed for the graphene edge procedure instead, albeit it might be more difficult to optically locate acceptable working areas on them.

In Figure 3, an AFM measurement of the edge employed throughout this work is reported. It shows that the edge was not greatly jagged and that the deviation from the average line (i.e., an ideal straight edge) was at most 10 nm in total for both sides; therefore, the maximum possible bias because of the jaggedness was estimated to be less than 10 nm. For a more ideal and controlled edge, nanopatterning techniques such as AFM lithography, electron beam lithography or focussed ion milling are recommended, but they were not deemed necessary for this work for the sake of simplicity, given the much higher expected dimensions of the confocal volumes. Another source of bias is undoubtedly the direction of the edge with respect of the scan line(s): if the two are not perpendicular with respect to one another, the width of the profile would be elongated by a factor of $\frac{1}{cos\theta}$, where θ is the angular offset from the orthogonality condition.

Data analysis was performed by measuring the Raman intensity of graphene along the scanning directions at appropriate intervals. In the DXRxi, step sizes of 0.1 μm in the planar directions and 0.2 μm in the axial direction were chosen because these were the minimum sizes allowed by the stage motors. For measurements on the DXR-Ntegra coupled setup, the piezoelectric stage had no such limitations, and step sizes of 100 and 200 nm were chosen in the planar and axial directions, respectively, to match with the DXRxi conditions.

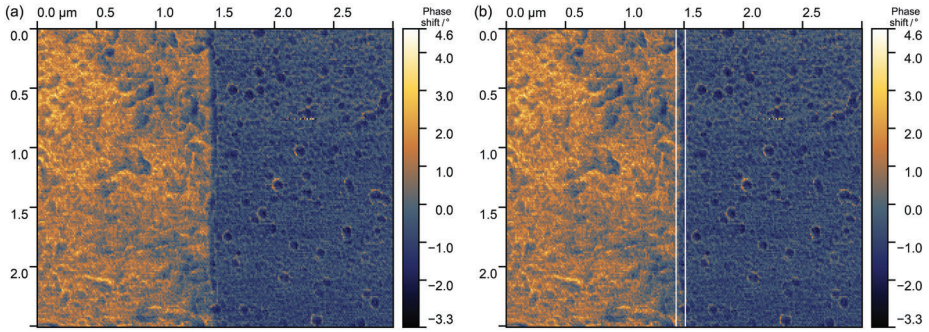

FIGURE 3 Phase-shift semi-contact AFM measurement of the graphene edge employed in this work. (a) Original measurement. (b) Measurement with superimposed white lines indicating the vertical position of the furthest deviations of the edge from the average. The distance between the two lines is 10 nm [Colour figure can be viewed at wileyonlinelibrary.com]

The intensity of the 2D Raman band of graphene at approximately 2670 cm^{-1} was the parameter of choice for describing the confocal volumes. Although the G band at about 1580 cm^{-1} could be employed instead, the 2D signal has several advantages: it is more intense than the G band in monolayer graphene, and it is much less prone to variation in its integral due to areas with multiple layers and does not split when the material is strained. Furthermore, the D band at approximately 1350 cm^{-1}, which arises exclusively where defects in the carbon lattice (which include the edges of the graphene flakes) are present, is close to the G peak and could negatively affect data analysis.[2,13,28]

The intensity of the graphene 2D signal was calculated from spectra after the application of the process described below on each spectrum. First, a linear baseline correction was calculated by best fitting a linear function to the spectral regions around the peak, excluding an interval of ± 25 cm^{-1} around the peak maximum, after Savitsky–Golay smoothing (first order, 15-point window). The resulting spectrum underwent least-square regression with a Lorentzian curve, as this is the expected shape of the 2D Raman band. The area under the function in an integration window of ± 25 cm^{-1} around the apex of the best-fit curve was then calculated and taken as the peak intensity and employed as a Raman intensity for the reported profiles.

To measure spatial features, data were treated as profiles of the Raman intensity as functions of lateral displacement of the graphene edge or the axial position of the full graphene sheet for lateral and axial profiles, respectively. Because the focal volume profiles were approximated as Gaussian curves, the measurements were best fitted with least-square regression with a standard Gaussian curve $G(z)$ for an axial profiling, and a modified Gauss error function $erf(x)$ for a lateral probing, because the profile in this case is a Gaussian cumulative function when measured with graphene edge. After regression, the data were centred and normalised with respect to the centre of symmetry and function maximum. From the best fit functions, the width parameters of the profiles were calculated, which alone characterise a normalised and centred Gaussian or Gauss error function.

All data analysis was performed with Python 3 programming language and its packages NumPy and SciPy. The Matplotlib library and Inkscape software were employed for data presentation and image construction in this paper.[48–50] The modified Gauss error function $erf(x)$ was a scaled and shifted version of the standard error function, which conventionally has co-domain $(-1; 1)$ when normalised, in order to yield the $(-\infty; x)$ integral of a Gaussian curve with varying intensity and width.

In this paper, the volumes were probed in three orthogonal directions: the axial direction z and two planar axes parallel to the motor stages native axes x and y. The number of lateral directions can be increased to more than two in order to describe the beam width more thoroughly or to accurately apply the method to diagonal raster scanning directions.

Images of the confocal volume of the DXRxi setup with the 532 nm laser as orthogonal projections in the xz and yz planes were taken with three-dimensional mapping by recording a series of planar (xy) scans with 0.2 µm spacing, each formed by two line scans with 0.2 µm pixel size. Gaussian kernel convolution on the images was applied for data presentation. The parameters for each spectrum were 1.0 mW laser power and 0.5 s integration time.

4 | RESULTS AND DISCUSSION

Table 1 summarises the widths of the profiles for the three configurations along three dimensions, depth (z) and two orthogonal planar directions (x and y). As

TABLE 1 Widths of the measured profiles for each configuration, expressed as full width at half maximum (FWHM) and as the total interval containing 95.5% of the total intensity (four times the Gaussian parameter σ)

Configuration	Axis	Confocal pinhole diameter	FWHM (nm)	95.5% interval 4σ (nm)	Number of samples
DXRxi (0.9 NA) 532 nm	x	50 μm	440 ($s = 43$)	748 ($s = 73$)	10
DXRxi (0.9 NA) 532 nm	y	50 μm	429 ($s = 26$)	729 ($s = 44$)	10
DXRxi (0.9 NA) 532 nm	z	50 μm	2,727 ($s = 67$)	4,633 ($s = 114$)	22
DXRxi (0.9 NA) 633 nm	x	50 μm	530 ($s = 47$)	900 ($s = 80$)	10
DXRxi (0.9 NA) 633 nm	y	50 μm	516 ($s = 46$)	877 ($s = 78$)	10
DXRxi (0.9 NA) 633 nm	z	50 μm	2,595 ($s = 124$)	4,409 ($s = 211$)	22
DXR-Ntegra (0.7 NA) 633 nm	x	50 μm	765 ($s = 35$)	1,300 ($s = 59$)	40
DXR-Ntegra (0.7 NA) 633 nm	y	50 μm	790 ($s = 41$)	1,342 ($s = 70$)	40
DXR-Ntegra (0.7 NA) 633 nm	z	50 μm	4,240 ($s = 180$)	7,204 ($s = 306$)	5
DXRxi (0.9 NA) 532 nm	z	50 μm	2,750 ($s = 70$)	4,672 ($s = 119$)	22
DXRxi (0.9 NA) 532 nm	z	25 μm	1,552 ($s = 62$)	2,637 ($s = 105$)	22

Note: Results are averages of multiple profiles least squares regressions; s indicates the standard deviation for the respective average.

previously discussed, several definitions of focal depth, spot size, beam waist and volume dimensions can be employed in order to describe the same profiles. In Table 1, two of these definitions, the full width at half maximum (FWHM) and 4σ, that is, four times the width parameter of the Gaussian profiles, corresponding to the profile width containing approximately 95.5% of the total curve integral, are used for the definition of the lateral dimensions for each set of measurements. Note that these values were calculated by Gaussian and Gauss error function best fits; therefore, the two values have the simple mathematical relationship: $4\sigma = 1.699 \times \text{FWHM}$. The DXRxi spectra with 633 nm excitation source were acquired with a laser power (measured at the stage) of $P = 3.0$ mW and exposure time of 5 s per pixel; when the 532 nm was employed on the same system, $P = 1.0$ mW and exposure times of 1 s per pixel were used. The DXR-Ntegra apparatus required a laser power at the stage of $P = 3.0$ mW and acquisition times of 10 s per point in planar profiles and 60 s for axial measurements to obtain comparable signal to noise ratios. Figure 4 shows some of the acquired profiles for the different configurations and Gaussian and Gauss error function least-square regressions for lateral and axial directions.

The measurements have shown similar values, well within the standard respective deviations, between the two axial directions of each configuration. Relative standard deviations were somewhat lower in the DXR-Ntegra apparatus, although not as much as expected. Because the authors believe that most of the internal variability in each data set was due to non-ideality of the stage and external vibrations, this is most likely imputable on the following factors. First, these measurements demonstrate lower signal to noise ratios with respect to the others due to lower efficiency of the optical apparatus (lower NA and higher radiation loss in the optical path). Furthermore, the scanning probe microscopy stage might not be able to adequately maintain a specific z coordinate, as this is constantly checked and corrected by probe feedback in normal operation; stage artefacts are also quite prominent in scans of lateral dimensions employed in this study. Moreover, the best-fit performances in the planar directions are different between the DXRxi and this apparatus: the scanning length of approximately 10 μm chosen for the DXRxi maps was beyond the maximum range of the Ntegra scanner, and at maximal range, the piezoelectric scan artefacts were very conspicuous. Therefore, a smaller profile length of 3 μm was employed

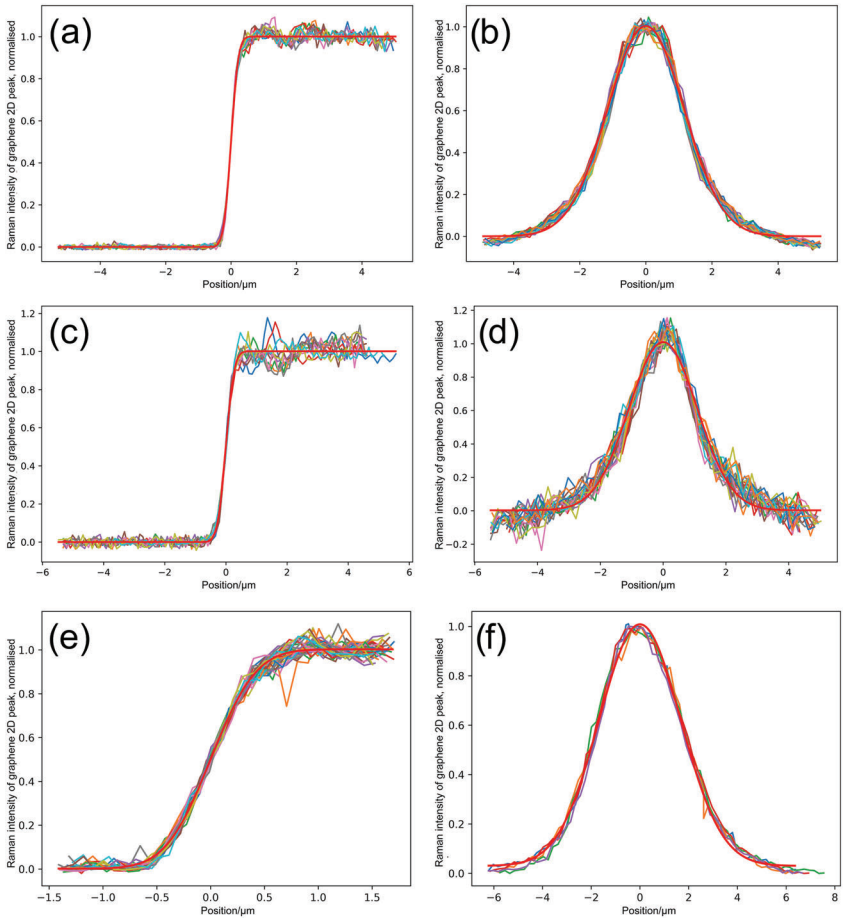

FIGURE 4 Raman intensity profiles measured with the graphene edge method in different configurations along radial and axial directions. (a,b) 532 nm laser, 0.9 NA. (c,d) 633 nm laser, 0.9 NA. (e,f) 633 nm, 0.7 NA. (a, c,e) planar profiles. (b,d,f) axial profiles. Red lines are least square regression curves on the whole respective dataset [Colour figure can be viewed at wileyonlinelibrary.com]

TABLE 2 Comparison of measured FWHMs with those theoretically expected by Rayleigh criterion

Configuration	Axis	Measured FWHM (nm)	Expected FWHM (nm)
DXRxi (0.9 NA) 532 nm	x	440 ($s = 43$)	361
DXRxi (0.9 NA) 532 nm	y	429 ($s = 26$)	361
DXRxi (0.9 NA) 532 nm	z	2,727 ($s = 67$)	1,314
DXRxi (0.9 NA) 633 nm	x	530 ($s = 47$)	429
DXRxi (0.9 NA) 633 nm	y	516 ($s = 46$)	429
DXRxi (0.9 NA) 633 nm	z	2,595 ($s = 124$)	1,563
DXR-Ntegra (0.7 NA) 633 nm	x	765 ($s = 35$)	552
DXR-Ntegra (0.7 NA) 633 nm	y	790 ($s = 41$)	552
DXR-Ntegra (0.7 NA) 633 nm	z	4,240 ($s = 180$)	2,584

Note: Results are averages of several profiles least squares regressions; s indicates the standard deviation for the respective average.

instead, effectively cropping out most of the two baselines in the Gauss error functions: this is noticeable while comparing the abscissae ranges in Figure 4a or c with Figure 4e.

Each result was considerably different from what could be predicted with the Rayleigh criterion for FWHM of the lateral profiles: $FWHM_{lateral} = \frac{0.61\lambda}{NA}$ and $FWHM_{axial} = \frac{2n\lambda}{NA^2}$, where λ is the radiation wavelength and n the refractive index of the medium.[24] These discrepancies, displayed in Table 2, were not surprising for reasons discussed previously and are the very reason because of which an empirical method to measure such profiles was sought and is advisable for quantitative Raman microscopy applications. Furthermore, the ratios between expected and measured lateral FWHMs in the DXRxi with the two wavelengths are compatible with each other, suggesting that the same factor impacts on the widths in each of these measurements.

Despite the systematic differences between theory and experimental results due to non-ideality of the systems, by comparing the planar FWHMs in the same apparatus with the two different excitation wavelengths used in this work, many empirical variables of difficult evaluation are eliminated, and conclusion on the consistency of the measurements can be drawn. The ratios of the FWHMs of the beams of the two wavelengths in the DXRxi were measured as $\frac{\mathrm{FWHM}_x(633\,\mathrm{nm})}{\mathrm{FWHM}_x(532\,\mathrm{nm})} = 1.20$ and $\frac{\mathrm{FWHM}_y(633\,\mathrm{nm})}{\mathrm{FWHM}_y(532\,\mathrm{nm})} = 1.20$ for the x and y axes, respectively, whereas the ratio of the values predicted with the Rayleigh criterion is $\frac{\mathrm{FWHM}_r(633\,\mathrm{nm})}{\mathrm{FWHM}_r(532\,\mathrm{nm})} = 1.19$, which is almost identical to the experimental values.

Such considerations are not applicable to the measured confocal depths, as Table 2 suggests. In fact, the average axial FWHM with the 532 nm laser is somewhat larger than the respective one with the 633 nm source, even though the behaviour should be the opposite.[23] However, every measurement in Table 2 was taken with a 50 μm diameter pinhole as a confocal aperture size. This aperture diameter is equal to approximately five radial optical units ($\mathrm{OU_{rad}}$) in these experimental conditions.[25] For such pinhole dimensions (>2.5 $\mathrm{OU_{rad}}$), it was found that radiation diffraction effects do not have a major impact on the confocal volume axial FWHM,[24,25] which could explain these findings. To verify this, a set of vertical graphene scans with the DXRxi and the 532 nm excitation line was performed with a confocal aperture size of 25 μm (approximately 2.5 $\mathrm{OU_{rad}}$), condition in which the diffractive effects are predicted to dominate the depth resolution of the microscope,[25] as well as another run with the 50 μm diameter pinhole to compare it with the aforementioned aperture. The results are shown in the last two rows of Table 1 and in Figure 5.

The ratio between the FWHMs with the two apertures is approximately 1.8, which is in line with data shown in previous studies [24,25,51] in these conditions. The following formula, derived from diffraction limits for axial and planar directions,[25] can be used to predict the ratio between predicted axial and radial FWHMs in a purely diffractive regime: $\frac{FWHM_z}{FWHM_r} = \frac{3.28n}{NA}$. In these conditions, the value is equal to 3.64. The empirically measured ratio between the $\mathrm{FWHM_z}$ with the 25 μm aperture and the average radial $\mathrm{FWHM_r}$ indeed amounts to 3.57, well within the range dictated by the standard deviations on the axial measurements: this is further confirmation of the consistency of the measurements acquired with the graphene edge method.

Another important properties of a Raman microscope, crucial to substance quantification, are the total sizes of the confocal volume and the laser spot area at the focus plane. With the information on the Raman intensity profiles in three orthogonal directions, with Gaussian approximations in every direction, and chosen the same intensity threshold with respect to the focal point for all directions, the isophote surface in three dimensions is an ellipsoid; therefore, its section at the focal plane is an ellipse. The confocal volumes and focus spot areas were calculated for the optical system illustrated earlier with the three sets of profiles shown, by considering the volume as an ellipsoid with semiaxes equal to the measured $2\sigma_i$, with $i = x, y, z$, using the geometrical formula $V = \frac{4}{3}\pi abc$, where a, b and c are the semiaxes of the ellipsoid. One of the chosen intensities threshold for the limits of the unidimensional profiles in this work shown so far was $1/e^2$ (13.5%) of the maximum, a widespread value employed in optics corresponding to a round value of $\pm 2\sigma$ in width and an integral of 95.5% of the total for a univariate Gaussian. It is worth noting that, if the definition of the lateral limit with the $1/e^2$ intensity threshold is applied to a three-dimensional Gaussian in each Cartesian direction, its integral inside that boundary surface is 73.9% of the total, whereas the same calculations for a two-dimensional Gaussian curve yields 86.5% of the total. In order to define the boundaries containing fractions of the total intensity closer to commonly accepted limits, different intensity thresholds and widths should be established according to the total contained areas or volumes. In Table 3, confocal volumes and focussed spot areas are reported, defined with ellipsoids and ellipses limits of axes lengths proportional to the σ_i determined earlier by factors that were deemed mnemonically convenient. Figure 6 shows renderings based on these limits applied to the DXR system. The uncertainties on the reported volumes and areas were determined with a coverage factor $k = 1.96$ from the standard deviations on the

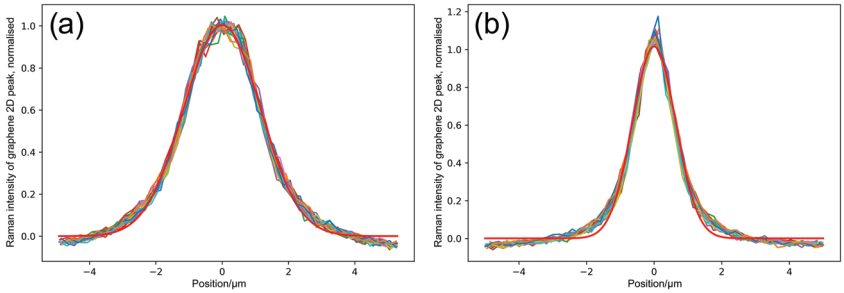

FIGURE 5 Axial Raman intensity profiles measured with the graphene method on the DXRxi setup (0.9 NA) with the 532 nm laser with different confocal apertures. (a): 50 μm diameter pinhole; (b) 25 μm diameter pinhole. Red lines indicate least square regression on the whole respective dataset [Colour figure can be viewed at wileyonlinelibrary.com]

TABLE 3 Spot size at the focal plane and confocal volumes calculated with ellipses and ellipsoids as limits, whose axes are proportional to the profile widths σ_i measured with the graphene edge method by different proportionality factors

Geometry and width definition	Area in $2\sigma_i$	Area in $2.145\sigma_i$	Area in $2.45\sigma_i$
Total radiation contained	86.5%	90.0%	95.0%
Intensity threshold	13.5% ($1/e^2$)	10.0%	5.0%
DXR-Ntegra (0.7 NA) 633 nm	(1.37 ± 0.15) μm^2	(1.58 ± 0.17) μm^2	(2.1 ± 0.2) μm^2
DXRxi (0.9 NA) 633 nm	(0.62 ± 0.12) μm^2	(0.71 ± 0.14) μm^2	(0.93 ± 0.18) μm^2
DXRxi (0.9 NA) 532 nm	(0.43 ± 0.08) μm^2	(0.49 ± 0.09) μm^2	(0.64 ± 0.11) μm^2
Geometry and width definition	**Volume in $2\sigma_i$**	**Volume in $2.5\sigma_i$**	**Volume in $2.8\sigma_i$**
Total radiation contained	73.9%	90.0%	95.1%
Intensity threshold	13.5% ($1/e^2$)	4.4%	2.0%
DXR-Ntegra (0.7 NA) 633 nm (50 μm pinhole)	(6.6 ± 0.5) μm^3	(12.9 ± 1.1) μm^3	(18.1 ± 1.5) μm^3
DXRxi (0.9 NA) 633 nm (50 μm pinhole)	(1.8 ± 0.3) μm^3	(3.6 ± 0.5) μm^3	(5.0 ± 0.7) μm^3
DXRxi (0.9 NA) 532 nm (50 μm pinhole)	(1.32 ± 0.16) μm^3	(2.6 ± 0.3) μm^3	(3.6 ± 0.4) μm^3
DXRxi (0.9 NA) 532 nm (25 μm pinhole)	(0.75 ± 0.09) μm^3	(1.47 ± 0.18) μm^3	(2.1 ± 0.3) μm^3

Note: In this notation, σ_i is measured in Cartesian directions from the centre; that is, for a unidimensional profile, the $2\sigma_i$ width limit would correspond to $\pm 2\sigma$ which was used in Table 1.

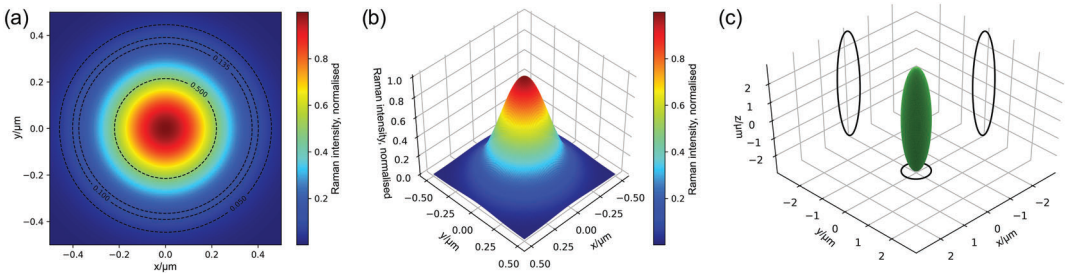

FIGURE 6 Renderings of measured laser spot and confocal volume of the DXRxi setup (0.9 NA) with 532 nm excitation wavelength and 50 μm confocal pinhole. (a) Raman intensity at the focal plane, with contour lines marking various possible intensity limits relative to the maximum for the definition of the spot size, namely, FWHM (0.500), 1/e2 (0.135) and the others considered in Table 3 (the numbers are expressed as fractions of maximum intensity). (b) Same rendering in 3D, with vertical axis showing Raman intensity. (c) Boundary surface containing 90% of total Raman intensity (width limit is 2.5si; threshold is 4.4% of the maximum signal) and the corresponding confocal volume of (2.6 ± 0.3) μm3, with depicted projections on the Cartesian planes [Colour figure can be viewed at wileyonlinelibrary.com]

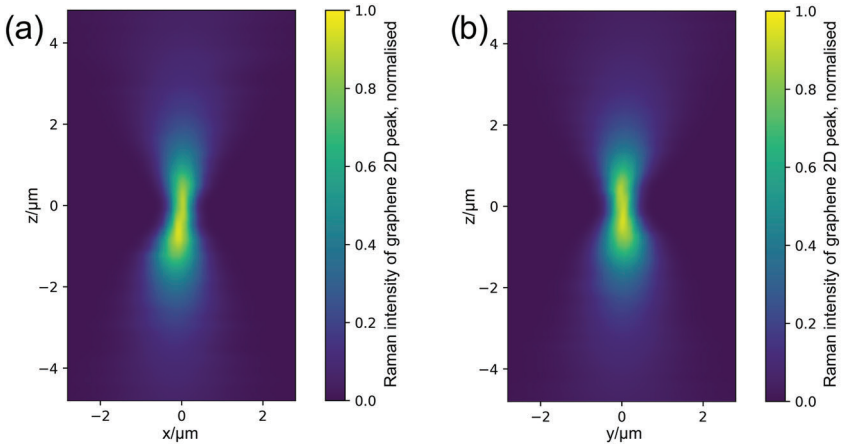

FIGURE 7 Measured projections of the Raman volume intensity on two orthogonal planes parallel to the optical axis *z*, achieved with the three-dimensional graphene edge scanning approach on the 532 nm laser, 0.9 NA, 50 μm confocal pinhole DXRxi system. (a) *xz* scan. (b) *yz* scan [Colour figure can be viewed at wileyonlinelibrary.com]

average profile widths measured with the graphene edge method.

Figure 7 shows the results of three-dimensional scans with the graphene edge method for the DXR setup with the 532 nm excitation laser and the 50 μm confocal pinhole, acquired by measuring radial profiles along multiple optical planes near the focal plane. This approach results in real two-dimensional images of the whole focal volume as projections on the plane formed by the fast and the slow scan directions after reconstructing the equivalent Gaussian profiles from the measured cumulative Gaussian profiles. Some degree of skewness can be observed with this method on both images: it was not possible to detect this with separate measurements for each Cartesian axis, but it was easily discovered with the three-dimensional approach. This behaviour can be attributable to imperfect optical alignment or microscope stage drift and could also explain the discrepancies between the theoretical predictions and the empirical measurements on the FWHMs shown in Table 2.

5 | CONCLUSIONS

The graphene edge method for the three-dimensional characterisation of the profile and the dimensions of Raman microscopes was proposed and experimentally applied to three different confocal setups, and the results were compared with theoretical expectations and with one another to check their consistency. The approach allowed the attainment of empirical information on the shape and size of the volume on several directions, both axial and radial, from which dimensional estimates on the volumes could be calculated with their relative uncertainties.

The measurements demonstrated some discrepancies between the expected and observed sizes, which could be explained by the non-ideality of the instrumentation, the alignment or the inapplicability of the hypotheses from which the equations were derived (i.e., a purely diffraction-limited system in the axial direction). Such disparities could not be predicted or quantified without empirical measurements. The results, summarised in Table 1, were checked for self-consistency with positive outcomes and appeared to be systematic, which is an indication of the reliability of the graphene edge technique. It was possible with this method to acquire a substantial sample size with relative ease and speed from which uncertainties on the measurands can be quantified in a simple way. With these data, the total confocal Raman volumes and focussed spot areas of the microscopes with various definitions could be calculated (see Table 3): with the definition of the confocal volume as the space containing 90% of the total intensity, it was found that the system with the 633 nm He-Ne excitation source and the 100 × LWD, 0.7 NA microscope objective had a Raman confocal volume of (12.9 ± 1.1) μm^3 with a 50 μm circular confocal aperture; it was determined that the apparatus with the 100X microscope objective with 0.9 NA had a focal volume of (3.6 ± 0.5) μm^3 with the 633 nm excitation laser (50 μm confocal pinhole), (2.6 ± 0.3) μm^3 with the frequency-doubled Nd:YAG 532 nm excitation source collected with a 50 μm confocal pinhole and (1.47 ± 0.18) μm^3 with the same laser and the 25 μm confocal aperture size.

A variant of the procedure was also presented, involving three-dimensional scanning and resulting in an actual 'side view' of the focal volume. Detection of evidences of skewness of the optical axis with respect to the microscope stage coordinates was possible with this approach, which could also be the cause of the deviations of the experimental profile results from theoretical calculations.

The graphene edge approach to Raman focal volume measurement employs an inexpensive probe with possibly atomic dimensions which is also very chemically and mechanically stable and with great Raman cross section.

The method could technically have nanometric accuracy with the appropriate consideration (microscopy stage and focussing method), and in practice, its precision is limited by the manufacturing process of the straight graphene edge itself and the technical characteristics and performance of the motor stage and the microspectrometer. In order to validate the graphene edge procedure, the next steps to take would be an interlaboratory comparison and the independent verification of confocal volumes measured with this method. This goal could be achieved, for instance, by employing molecules with known absolute Raman cross sections and acquiring their spectra in transparent liquid (pure or in solution) and comparing them with the Raman intensities expected from their cross sections and the predicted amounts of substance, calculated by using their densities/concentrations and the confocal volume information. Profile data acquired with these measurements have considerable applications in quantitative Raman microscopy imaging; moreover, accurate Raman volume determination is fundamental in pursuing absolute chemical quantification with Raman spectroscopy, and the graphene edge method is a new approach towards this much-sought objective.

ACKNOWLEDGEMENTS

The present work has been supported by the project "ISO-G-SCoPe." This project 19NRM04 ISO-G-SCoPe has received funding from the EMPIR programme co-financed by the Participating States and from the European Union's Horizon 2020 research and innovation programme.

DATA AVAILABILITY STATEMENT

The data that support the findings of this study are available from the corresponding author upon reasonable request.

ORCID

Alessio Sacco https://orcid.org/0000-0003-4421-840X

REFERENCES

[1] H. J. Butler, L. Ashton, B. Bird, G. Cinque, K. Curtis, J. Dorney, K. Esmonde-White, N. J. Fullwood, B. Gardner, P. L. Martin-Hirsch, M. J. Walsh, M. R. McAinsh, N. Stone, F. L. Martin, *Nat. Protoc.* **2016**, *11*, 664. https://doi.org/10.1038/nprot.2016.036

[2] J. B. Wu, M. L. Lin, X. Cong, H. N. Liu, P. H. Tan, *Chem. Soc. Rev.* **2018**, *47*, 1822.

[3] W. Zhang, J. Ma, D. W. Sun, *Crit. Rev. Food Sci. Nutr.* **2020**, 1.

[4] D. W. Shipp, F. Sinjab, I. Notingher, *Adv Opt Photonics* **2017**, *9*, 315.

[5] C. Portesi, D. Visentin, F. Durbiano, M. C. Abete, M. Rizzi, V. Maurino, A. M. Rossi, *Polym. Test.* **2019**, *80*, 106098. https://doi.org/10.1016/j.polymertesting.2019.106098

[6] G. M. do Nascimento, *Raman Spectroscopy*, BoD–Books on Demand, Norderstedt, Germany **2018**.

[7] G. Barzan, A. Sacco, L. Mandrile, A. M. Giovannozzi, J. Brown, C. Portesi, M. R. Alexander, P. Williams, K. R. Hardie, A. M. Rossi, *Sens. Actuators, B* **2020**, *309*, 127774. https://doi.org/10.1016/j.snb.2020.127774

[8] W. Österle, A. Giovannozzi, T. Gradt, I. Häusler, A. Rossi, B. Wetzel, G. Zhang, A. I. Dmitriev, *Tribol. Int.* **2015**, *90*, 481.

[9] M. Sackmann, A. Materny, *J. Raman Spectrosc.* **2006**, *37*, 305.

[10] E. Cara, L. Mandrile, F. Ferrarese Lupi, A. M. Giovannozzi, M. Dialameh, C. Portesi, K. Sparnacci, N. de Leo, A. M. Rossi, L. Boarino, *Sci. Rep.* **2018**, *8*, 1.

[11] A. D'Agostino, A. M. Giovannozzi, L. Mandrile, A. Sacco, A. M. Rossi, A. Taglietti, *Talanta* **2020**, *216*, 120936.

[12] L. Mandrile, I. Cagnasso, L. Berta, A. M. Giovannozzi, M. Petrozziello, F. Pellegrino, A. Asproudi, F. Durbiano, A. M. Rossi, *Food Chem.* **2020**, *326*, 127009.

[13] Y. Kim, E. J. Lee, S. Roy, A. S. Sharbirin, L.-G. Ranz, T. Dieing, J. Kim, *Curr. Appl. Phys.* **2020**, *20*, 71.

[14] Y. Maruyama, W. Kanematsu, *J. Appl. Phys.* **2011**, *110*, 103107.

[15] C. Coman, L. F. Leopold, *Raman Spectroscopy and Applications*, IntechOpen, Rijeka, Croatia **2017**.

[16] P. Rösch, M. Harz, M. Schmitt, K. D. Peschke, O. Ronneberger, H. Burkhardt, H. W. Motzkus, M. Lankers, S. Hofer, H. Thiele, J. Popp, *Appl. Environ. Microbiol.* **2005**, *71*, 1626.

[17] P. Worsfold, A. Townshend, C. F. Poole, M. Miró, *Encyclopedia of Analytical Science*, Elsevier, Amsterdam, Netherlands **2019**.

[18] L. Mandrile, A. M. Giovannozzi, A. Sacco, G. Martra, A. M. Rossi, *Biosensors* **2019**, *9*, 145.

[19] E. Cara, L. Mandrile, A. Sacco, A. M. Giovannozzi, A. M. Rossi, F. Celegato, N. de Leo, P. Hönicke, Y. Kayser, B. Beckhoff, D. Marchi, A. Zoccante, M. Cossi, M. Laus, L. Boarino, F. Ferrarese Lupi, *J. Mater. Chem. C* **2020**, *8*, 16513.

[20] L. Mandrile, A. M. Giovannozzi, F. Durbiano, G. Martra, A. M. Rossi, *Food Chem.* **2018**, *224*, 16.

[21] JCFGIM JCGM, International Organization for Standardization Geneva ISBN.

[22] Chemistry International. Newsmagazine for IUPAC, DOI: https://doi.org/10.1515/ci.2008.30.6.21

[23] M. Born, E. Wolf, E. Hecht, *Principles of Optics: Electromagnetic Theory of Propagation, Interference and Diffraction of Light*. 7th ed., Cambridge University Press, Cambridge, United Kingdom **1999**.

[24] M. Mueller, *Introduction to Confocal Fluorescence Microscopy*, 2nd ed., SPIE Press, Bellingham, Washington, USA **2010**.

[25] J. B. Pawley, *Handbook of Biological Confocal Microscopy*, Third ed., Springer, Boston, MA **2008**.

[26] A. C. Ferrari, D. M. Basko, *Nat. Nanotechnol.* **2013**, *8*, 235.

[27] V. L. Mironov, *Fundamentals of Scanning Probe Microscopy*, The Russian Academy of Sciences Institute of Physics of Microstructures, Nizhniy Novgorod, Russia **2004**.

[28] C. Korzeniewski, J. P. Kitt, S. Bukola, S. E. Creager, S. D. Minteer, J. M. Harris, *Anal. Chem.* **2019**, *9*, 1049.

[29] M. C. M. Moya Moreno, D. Mendoza Olivares, F. J. Amézquita López, J. V. Gimeno Adelantado, F. Bosch Reig, *J. Mol. Struct.* **1999**, *482*, 551.

[30] ISO, BS ISO 18337: **2015**.

[31] ISO18516. 2019, **2019**, *9*, 40.

[32] J. Adler, S. N. Pagakis, *J Microsc* **2003**, *210*, 131.

[33] R. Mcgorty, D. Kamiyama, B. Huang, *Opt Nanoscopy* **2013**, *2*, 3.
[34] R. R. Nair, P. Blake, A. N. Grigorenko, K. S. Novoselov, T. J. Booth, T. Stauber, N. M. R. Peres, A. K. Geim, *Science* **2008**, *320*, 1308.
[35] M. Bruna, *Study of Graphene for the Realization of Optimezed Graphene-Based Electronic Devices*, PhD thesis, Politecnico di Torino, Turin, Italy **2011**.
[36] A. Rzhevskii, Spectroscopy (Santa Monica) **2016**, *31*, 40.
[37] D. R. Skinner, R. E. Whitcher, *J. Phys. E: Sci. Instrum.* **1972**, *5*, 237. https://doi.org/10.1088/0022-3735/5/3/015
[38] O. Svelto, *Principles of lasers*, Springer, New York **2010**.
[39] S. Weisenburger, V. Sandoghdar, *Contemp. Phys.* **2015**, *56*, 123. https://doi.org/10.1080/00107514.2015.1026557
[40] T. Latychevskaia, *Appl. Opt.* **2019**, *58*, 3597.
[41] D. van de Sompel, E. Garai, C. Zavaleta, S. S. Gambhir, Single Molecule Spectroscopy and Superresolution Imaging VI, Vol. *8590* **2013** p. 85900I-undefined. Comparison of Gaussian and Poisson noise models in a hybrid reference spectrum and principal component analysis algorithm for Raman spectroscopy, 85900.I
[42] S. J. Barton, T. E. Ward, B. M. Hennelly, *Anal. Methods* **2018**, *10*, 3759.
[43] G. B. Airy, *Trans. Camb. Phil. Soc.* **1835**, *5*, 287.
[44] R. Zhang, Y. Zhang, Z. C. Dong, S. Jiang, C. Zhang, L. G. Chen, L. Zhang, Y. Liao, J. Aizpurua, Y. Luo, J. L. Yang, J. G. Hou, *Nature* **2013**, *498*, 82.
[45] A. Sacco, D. Imbraguglio, A. M. Giovannozzi, C. Portesi, A. M. Rossi, *RSC Adv.* **2018**, *8*, 27863. https://doi.org/10.1039/c8ra03762k
[46] A. Sacco, S. Mangino, C. Portesi, E. Vittone, A. M. Rossi, *J. Phys. Chem. C* **2019**, *123*, 24723. https://doi.org/10.1021/acs.jpcc.9b07016
[47] H. Park, C. Lim, C. J. Lee, J. Kang, J. Kim, M. Choi, H. Park, *Nanotech.* **2018**, *29*, 415303. https://doi.org/10.1088/1361-6528/aad4d9
[48] C. R. Harris, K. J. Millman, S. J. van der Walt, R. Gommers, P. Virtanen, D. Cournapeau, E. Wieser, J. Taylor, S. Berg, N. J. Smith, R. Kern, M. Picus, S. Hoyer, M. H. van Kerkwijk, M. Brett, A. Haldane, J. F. del Río, M. Wiebe, P. Peterson, P. Gérard-Marchant, K. Sheppard, T. Reddy, W. Weckesser, H. Abbasi, C. Gohlke, T. E. Oliphant, *Nature* **2020**, *585*, 357.
[49] P. Virtanen, R. Gommers, T. E. Oliphant, M. Haberland, T. Reddy, D. Cournapeau, E. Burovski, P. Peterson, W. Weckesser, J. Bright, S. J. van der Walt, M. Brett, J. Wilson, K. J. Millman, N. Mayorov, A. R. J. Nelson, E. Jones, R. Kern, E. Larson, C. J. Carey, İ. Polat, Y. Feng, E. W. Moore, J. VanderPlas, D. Laxalde, J. Perktold, R. Cimrman, I. Henriksen, E. A. Quintero, C. R. Harris, A. M. Archibald, A. H. Ribeiro, F. Pedregosa, P. van Mulbregt, A. Vijaykumar, A. Pietro Bardelli, A. Rothberg, A. Hilboll, A. Kloeckner, A. Scopatz, A. Lee, A. Rokem, C. N. Woods, C. Fulton, C. Masson, C. Häggström, C. Fitzgerald, D. A. Nicholson, D. R. Hagen, D. V. Pasechnik, E. Olivetti, E. Martin, E. Wieser, F. Silva, F. Lenders, F. Wilhelm, G. Young, G. A. Price, G. L. Ingold, G. E. Allen, G. R. Lee, H. Audren, I. Probst, J. P. Dietrich, J. Silterra, J. T. Webber, J. Slavič, J. Nothman, J. Buchner, J. Kulick, J. L. Schönberger, J. V. de Miranda Cardoso, J. Reimer, J. Harrington, J. L. C. Rodríguez, J. Nunez-Iglesias, J. Kuczynski, K. Tritz, M. Thoma, M. Newville, M. Kümmerer, M. Bolingbroke, M. Tartre, M. Pak, N. J. Smith, N. Nowaczyk, N. Shebanov, O. Pavlyk, P. A. Brodtkorb, P. Lee, R. T. McGibbon, R. Feldbauer, S. Lewis, S. Tygier, S. Sievert, S. Vigna, S. Peterson, S. More, T. Pudlik, T. Oshima, T. J. Pingel, T. P. Robitaille, T. Spura, T. R. Jones, T. Cera, T. Leslie, T. Zito, T. Krauss, U. Upadhyay, Y. O. Halchenko, Y. Vázquez-Baeza, *Nat. Methods* **2020**, *17*, 261.
[50] E. Jones, T. Oliphant, P. Peterson, Others, SciPy.org.
[51] H. T. M. van der Voort, G. J. Brakenhoff, *J. Microsc.* **1990**, *158*, 43.

How to cite this article: A. Sacco, C. Portesi, A. M. Giovannozzi, A. M. Rossi, *J Raman Spectrosc* **2021**, 1. https://doi.org/10.1002/jrs.6187